LUND UNIVERSITY

Recent divergence in the contributions of tropical and boreal forests to the terrestrial carbon sink

Tagesson, Torbern; Schurgers, Guy; Horion, Stéphanie; Ciais, Philippe; Tian, Feng; Brandt, Martin; Ahlström, Anders; Wigneron, Jean Pierre; Ardö, Jonas; Olin, Stefan; Fan, Lei; Wu, Zhendong; Fensholt, Rasmus

LUND UNIVERSITY

PO Box 117
221 00 Lund
+46 46-222 00 00

Recent divergence in the contributions of tropical and boreal forests to the terrestrial carbon sink

Torbern **Tagesson**[1,2]*, Guy **Schurgers**[2], Stephanie **Horion**[2], Philippe **Ciais**[3], Feng **Tian**[1], Martin **Brandt**[2], Anders **Ahlström**[1,4], Jean-Pierre **Wigneron**[5], Jonas **Ardö**[1], Stefan **Olin**[1], Lei **Fan**[5,6], Zhendong **Wu**[1] and Rasmus **Fensholt**[2]

Anthropogenic land use and land cover changes (LULCC) have a large impact on the global terrestrial carbon sink, but this effect is not well characterized according to biogeographical region. Here, using state-of-the-art Earth observation data and a dynamic global vegetation model, we estimate the impact of LULCC on the contribution of biomes to the terrestrial carbon sink between 1992 and 2015. Tropical and boreal forests contributed equally, with the largest share of the mean global terrestrial carbon sink. CO_2 fertilization was found to be the main driver increasing the terrestrial carbon sink from 1992 to 2015, but the net effect of all drivers (CO_2 fertilization and nitrogen deposition, LULCC and meteorological forcing) caused a reduction and an increase, respectively, in the terrestrial carbon sink for tropical and boreal forests. These diverging trends were not observed when applying a conventional LULCC dataset, but were also evident in satellite passive microwave estimates of aboveground biomass. These datasets thereby converge on the conclusion that LULCC have had a greater impact on tropical forests than previously estimated, causing an increase and decrease of the contributions of boreal and tropical forests, respectively, to the growing terrestrial carbon sink.

Terrestrial vegetation globally absorbs 30% of the anthropogenic CO_2 emissions on average, representing an important ecosystem service mitigating climate change[1]. The exchange of carbon between terrestrial ecosystems and the atmosphere is a delicate balance between large exchange processes, and a change in any of these can have a substantial impact on the dynamics of this relatively small net exchange. An improved understanding of the processes affecting the net terrestrial carbon exchange is therefore essential to better understand, quantify and forecast the effects of current and future climate change, and is of relevance for climate change mitigation policies designed to reduce atmospheric CO_2.

Major knowledge gaps remain regarding the regional distribution of the global terrestrial carbon sink. Inventories and results from a process-based model suggest that the majority of carbon sequestered by the terrestrial biosphere has been accumulated in forest ecosystems, primarily in the tropics[2,3]. Measurements of the interhemispheric gradient of atmospheric CO_2 indicate an increasing northern terrestrial sink from the 1960s to the present day, with an acceleration since the 1990s[4]. In the tropics, atmospheric CO_2 inversions and biomass change—deduced from optical remote sensing data—indicate carbon neutrality or even a large net source of carbon[5–9]. Reducing the uncertainty of the estimates is essential to resolve these discrepancies, and combining Earth observation data with global-scale modelling can lead to an improved understanding of the regional distribution within the global terrestrial carbon sink[7].

Global human population growth and thus increased food and fibre consumption increase the appropriation of net primary production[10], with profound consequences on ecosystems structure and function[11,12]. LULCC are particularly ubiquitous, since human management impacts about 80% of all ice-free land, replacing natural ecosystems with agricultural land and managed forests[13]. LULCC can alter the net terrestrial carbon exchange in both positive and negative directions, but in the past few decades has been dominated by deforestation, which causes carbon emissions and a loss in sink capacity as a result of accelerated carbon turnover[14]. LULCC is therefore the second largest source of anthropogenic carbon emission to the atmosphere, and represents about one third of the total accumulated anthropogenic carbon emissions since 1850[1]. Given the importance of LULCC within the global net terrestrial carbon exchange, spatially-explicit observation-based datasets are essential for improved estimates of the impact of LULCC on the net terrestrial carbon exchange.

The dynamic global land cover dataset from the European Space Agency (ESA) Climate Change Initiative (CCI) is a recent detailed time series of land cover for 1992–2015 based on state-of-the-art moderate resolution Earth observation data[15–17]. The correspondence between satellite land cover classes and plant functional types provides an opportunity to use these data to constrain a dynamic global vegetation model (DGVM) to calculate regional distribution of carbon sinks and sources. Additionally, direct Earth observation-based estimates of aboveground biomass (AGB) can be derived from satellite passive microwaves, with the strong advantage that they remain sensitive to biomass variations at biomass densities when optical-based products saturate[18,19]. AGB estimates from X-, C- and K-band vegetation optical depth (VOD-AGB) are available for 1993–2012[18], whereas the L-band VOD data (L-VOD) are available from 2010 from the Soil Moisture and Ocean Salinity (SMOS) mission[20,21]. In this study, we analyse the contribution of biomes to

[1]Department of Physical Geography and Ecosystem Science, Lund University, Lund, Sweden. [2]Department of Geosciences and Natural Resource Management, University of Copenhagen, Copenhagen, Denmark. [3]Laboratoire des Sciences du Climat et de l'Environnement, IPSL, Gif-sur-Yvette, France. [4]Center for Middle Eastern Studies, Lund University, Lund, Sweden. [5]Interactions Sol Plante Atmosphére, INRA, Université Bordeaux, Bordeaux, France. [6]Collaborative Innovation Center on Forecast and Evaluation of Meteorological Disaster, School of Geographical Sciences, Nanjing University of Information Science and Technology, Nanjing, China. *e-mail: torbern.tagesson@nateko.lu.se
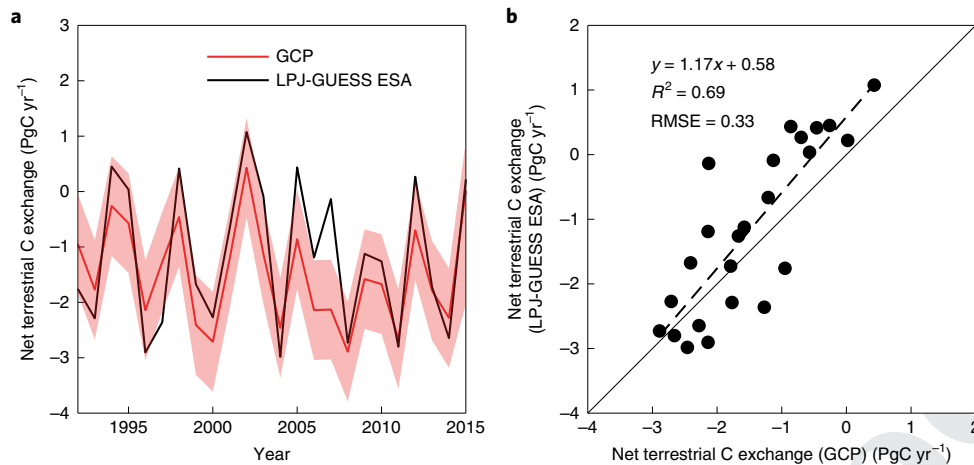
Fig. 1 | Agreement between the global net terrestrial carbon (C) exchange as estimated by the LPJ-GUESS model with the ESA-CCI dataset and as estimated by the multi-model mean of the GCP. a, Time series for 1992–2015, with s.d. (shaded area) estimated from the model ensemble GCP budgets of 0.9 PgC yr⁻¹ (ref. [1]). **b**, Interannual variability in the global net terrestrial carbon exchange as simulated by the LPJ-GUESS model with the ESA-CCI dataset versus multi-model mean estimates of the GCP. Agreement is quantified using an ordinary least-squares linear regression (dotted line). For a comparison with the atmospheric budget of the GCP, see Supplementary Fig. 7. RMSE, root mean square error.

the global terrestrial carbon sink 1992–2015 by combining Earth observation of land cover change with a DGVM, and by an independent assessment using the VOD-AGB and L-VOD datasets.

Results

We divided the Earth land surface into ten biomes on the basis of static main Köppen climate classes (tropical (A), arid (B), temperate (C), boreal (D) and polar (E))[22] and ESA-based dynamic vegetation types (Supplementary Fig. 1 and Supplementary Tables 1 and 2). These biomes included bare land, sparse vegetation, tundra, boreal low vegetation (low vegetation being areas with less than 15% herbaceous, crop, shrublands or woody cover), boreal forests, temperate low vegetation, temperate forests, semi-arid regions, tropical low vegetation and tropical forests. The contribution of the different biomes to the global carbon dynamics for 1992–2015 was analysed by using the DGVM Lund–Potsdam–Jena General Ecosystem Simulator (LPJ-GUESS)[23] constrained by annual fractions of woody and herbaceous cover derived from the land cover classes in the ESA-CCI annual land cover dataset 1992–2015[15,17] (Supplementary Information, subsection 1). This LPJ-GUESS simulation gives a global terrestrial carbon sink (sink and source represented as negative and positive values, respectively) of −1.15 ± 1.30 PgC yr⁻¹ (± s.d. of interannual variability) for 1992–2015. This is in the lower end, but still consistent with, a multi-model mean from the Global Carbon Project (GCP) which provides an estimate of −1.48 ± 0.92 PgC yr⁻¹ (Fig. 1; for a comparison against the GCP atmospheric budget, see Supplementary Fig. 7)[1]. The interannual variability in these two datasets also showed strong agreement (Fig. 1) and the trends in the total contribution of the land without the LULCC emissions were also similar (Supplementary Information, subsection 2.2).

We partitioned the DGVM-derived AGB and VOD-AGB[18] of terrestrial ecosystems into the different biomes and analysed their contribution to the mean global AGB for 1993–2012. The biomes with largest contribution were tropical and boreal forests, together accounting for approximately 60% of global AGB (Fig. 2a). Tropical forests showed a decrease and boreal forests showed an increase in their contribution to global AGB (Fig. 2b,c), whereas other biomes had relatively flat trends (Supplementary Fig. 9). The DGVM-derived AGB trends are in very good agreement with the VOD-AGB data (Fig. 2). Additionally, we compared the DGVM-derived AGB with L-VOD for 2011–2015[21]. The L-VOD time series is too

short to draw firm conclusions, but the trends for 2011–2015 in the two datasets showed good agreement (Fig. 2 and Supplementary Fig. 10).

Next, we applied the same partitioning into biomes for the DGVM-derived net carbon exchange and analysed their contributions to the mean, trends and interannual variability of the global terrestrial carbon sink for 1992–2015. The strongest contributors to the mean global terrestrial carbon sink for 1992–2015 were boreal forests (0.31 ± 0.19 PgC yr⁻¹, 28.1 ± 16.7%) and tropical forests (0.30 ± 0.37 PgC yr⁻¹, 26.9 ± 31.8%) (Fig. 3a and Supplementary Table 4). All other biomes showed relatively small contributions (between 0.8 and 11.1%) (Supplementary Fig. 4 and Supplementary Table 4). Although the definition of drylands used in this analysis has a lower spatial extent than the definition of semi-arid ecosystems by Ahlström et al.[3], our results support the conclusion that drylands were the biome that contributed most to the interannual variability (22.2 ± 5.8%) (Fig. 3b and Supplementary Table 4). Boreal forests exhibited the strongest sink trend and thereby also the largest contribution to the trend in the global terrestrial carbon sink for 1992–2015, with 29.6 ± 23.3% (Fig. 3c–e and Supplementary Table 4). Temporal changes in the contribution of biomes to the global terrestrial carbon sink showed an increasing and decreasing contribution of boreal and tropical forests, respectively (Fig. 3d,e).

There is a large interannual variability in the net terrestrial carbon exchange of tropical forests (Fig. 3d), causing a wide confidence interval for the estimated trends (Supplementary Table 4). However, in the tropics, a substantial fraction of interannual variability is caused by El Niño and La Niña events (Supplementary Fig. 6), and when removing variability caused by these events, trends for the tropical and boreal biomes remained similar (Supplementary Fig. 6). The tropical forests depicted carbon sources in 1998, 2005 and 2015. The years 1998 and 2015 were characterized by strong El Niño events, whereas the carbon source in 2005 was due to a drought in the Amazon basin and a carbon source from the Congo basin, caused by a warm subtropical North Atlantic Ocean[24]. In 2010, there were also severe droughts in the Amazon basin[25] causing a substantial reduction in the sink strength for this year, but on a global scale, this effect was compensated by a large sink in tropical forests of Africa and Asia.

To better understand the relative role of environmental drivers and LULCC causing the diverging trends of boreal and tropical
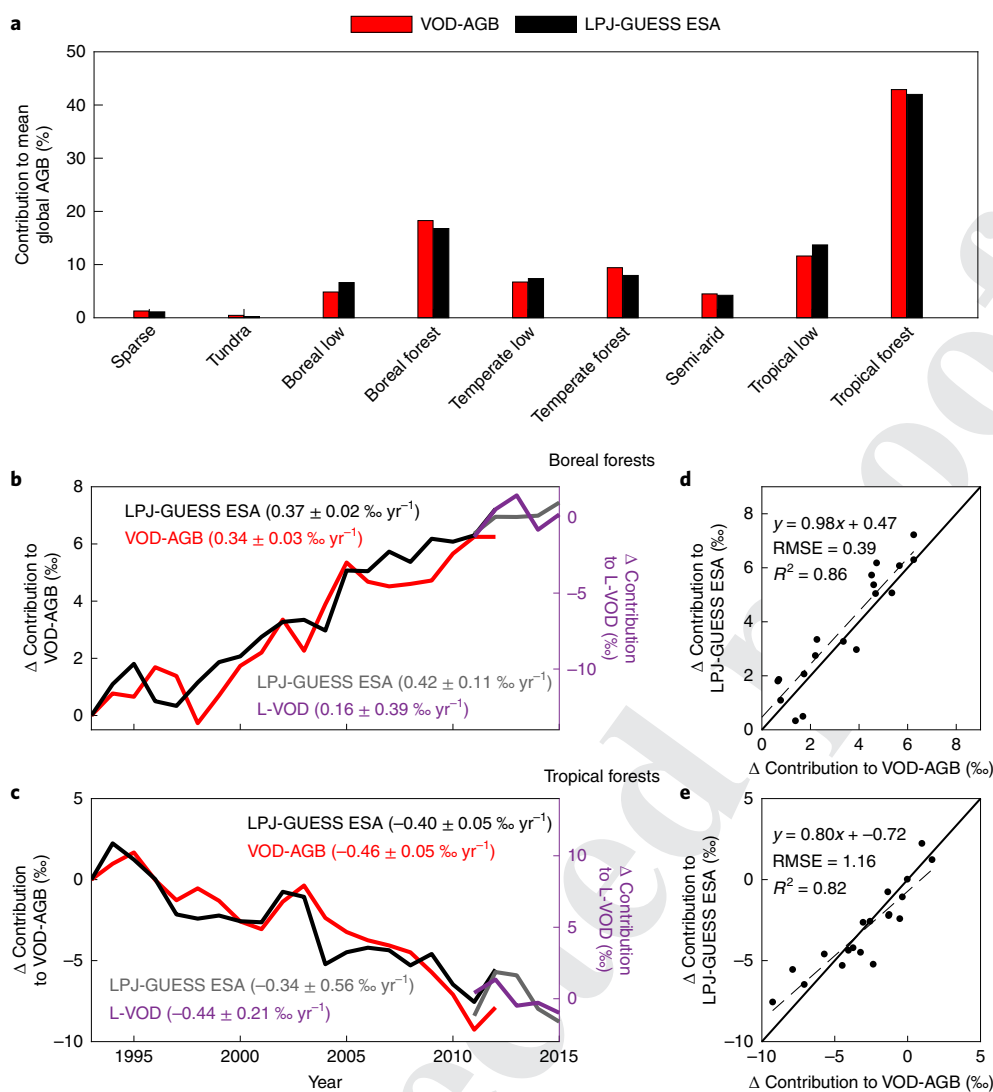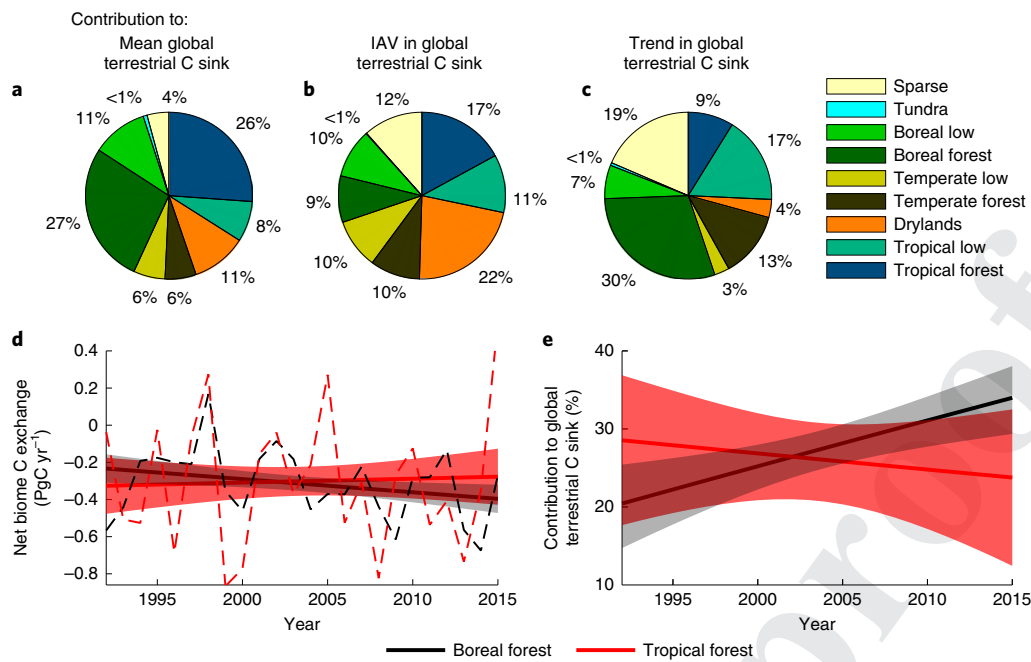
Fig. 2 | Contribution of biomes to AGB. a, Contribution of biomes to VOD-AGB and from LPJ-GUESS simulations with the ESA-CCI. **b,c**, Net changes in biome contribution to global-scale AGB for boreal (**b**) and tropical forests (**c**) for 1993–2015. Net changes in biome contribution relative to 1993 for LPJ-GUESS with ESA-CCI (black) and for VOD-AGB (red), and relative to average 2011–2015 for LPJ-GUESS with ESA-CCI (grey) and for L-VOD (purple). Ordinary least-squares linear regression trends 1993–2012 are shown brackets. **d,e**, Agreement in net changes in biome contribution to global-scale AGB 1993–2012 between LPJ-GUESS with ESA-CCI and the VOD-AGB for boreal (**d**) and tropical forests (**e**). The agreement is also quantified using an ordinary least-squares linear regression (dotted line).

forests in the global terrestrial carbon sink, we conducted factorial model simulations by separating the effects of (1) meteorological forcing, (2) increased atmospheric CO_2 concentrations and nitrogen deposition and (3) LULCC on both the simulated global- and biome-level carbon sinks. Those simulations showed that meteorological forcing and LULCC resulted in a carbon release to the atmosphere (globally on average, 0.42 ± 1.21 and 0.24 ± 0.12 PgC yr^{-1} during 1992–2015, respectively), whereas the increased atmospheric CO_2 concentrations and nitrogen deposition increased the terrestrial carbon sink (globally on average, -0.80 ± 0.39 PgC yr^{-1} during 1992–2015) (Fig. 4a). This was primarily caused by the increased CO_2 concentration and to a much lesser extent because of increased nitrogen deposition (Supplementary Fig. 11).

Tropical forests were the biome most strongly influenced by all three drivers (Fig. 4b), yet the effects of drivers in positive and negative directions nearly cancelled out (Fig. 4b). Even though our simulations indicate that tropical forests had a decreasing contribution to the global terrestrial carbon sink, it is evident that the high

sensitivities to individual drivers (Fig. 4b) result in uncertainties of the overall role of tropical forests. For boreal forests, however, an increased carbon sink caused by LULCC in this biome could be expected, given the substantial increase in forested area over the study period (Supplementary Fig. 1). At the same time, woody cover decreased for some regions in the boreal zone (Supplementary Fig. 1 and 2), generating small but positive net LULCC emissions (Fig. 4c and Supplementary Information, subsection 2.1). Therefore, both LULCC and meteorological forcing had minor roles in the trend in the boreal forests carbon sink for 1992–2015, whereas increased atmospheric CO_2 concentrations increased this sink considerably (Fig.4c). As a result, in sum, boreal forests were found to be the biome contributing most strongly to the trend in the global terrestrial carbon sink for 1992–2015 (Fig. 3e).

To assess the extent to which these results are specific for the DGVM LPJ-GUESS or the land use dataset, we compared the LPJ-GUESS simulations forced with the ESA-CCI annual land cover dataset with simulations from four of the DGVMs in the

Fig. 3 | Contributions of biomes to the global terrestrial carbon sink for 1992–2015. a–c, Contributions of biomes to: mean (**a**), interannual variability (IAV) (**b**) and trend (**c**) in the global terrestrial carbon sink for 1992–2015. Supplementary Table 4 shows the s.d. based on the interannual variability. **d,e,** Change in biome-level net terrestrial carbon exchange (**d**) and contribution to the global terrestrial carbon sink (**e**) for 1992–2015 for the boreal and tropical forests. The shaded area shows the region within 1× s.d. of the prediction interval. Contribution and net terrestrial carbon exchange of the other biomes is given in Supplementary Table 4 and Supplementary Fig. 4.
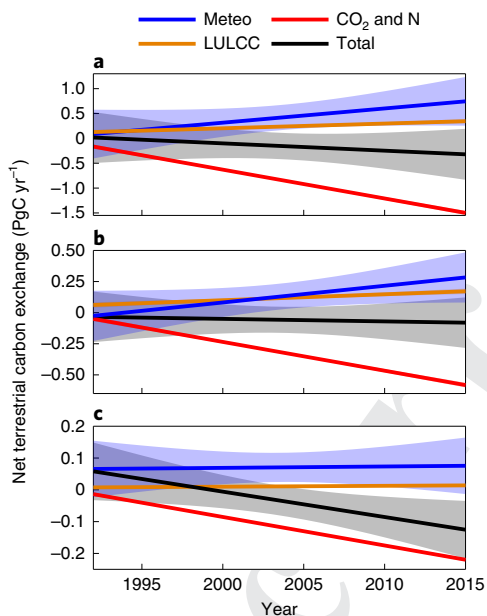
Fig. 4 | Impact of drivers on the trends in the net terrestrial carbon exchange. a–c, The impact is aggregated for boreal forests (**a**), tropical forests (**b**) and at the global scale (**c**). Included are: changes in net terrestrial carbon exchange for 1992–2015 as an effect of meteorological forcing (Meteo; air temperature, precipitation and cloudiness), increased atmospheric CO_2 concentrations and nitrogen deposition effects (CO_2 and N), LULCC, and all effects combined (Total). The shaded area shows the region within 1× s.d. of the prediction interval.

TRENDY v.5 model ensemble[26,27] (see methods), and simulations of LPJ-GUESS forced with the default LULCC dataset applied to TRENDY models, known as the land use harmonization dataset v.2

(LUH2)[28]. The TRENDY models are similarly forced by historical climate, atmospheric CO_2 data and the LUH2 LULCC data. For all biomes except the tropical forests, all model simulations (TRENDY, LPJ-GUESS ESA-CCI and LPJ-GUESS LUH2) showed biome contributions and trends similar to those in the VOD-AGB (Fig. 5a and Supplementary Fig. 9). For tropical forests, the VOD-AGB and LPJ-GUESS simulations forced with the ESA-CCI annual land cover dataset showed a strongly decreasing trend, whereas the TRENDY simulations and the LPJ-GUESS forced with LUH2 showed a flat trend (Fig. 5b). Again, the time series of the L-VOD dataset is too short to draw firm conclusions, but the comparison between trends for 2011–2015 indicate that the LPJ-GUESS simulations forced with the ESA-CCI annual land cover dataset were in better agreement with L-VOD than LPJ-GUESS and TRENDY simulations forced with LUH2 (Fig. 5c,d and Supplementary Fig. 10).

To conclude, when the same LULCC dataset is used, LPJ-GUESS shows similar results to the TRENDY models; however, with the Earth observation-based ESA-CCI LULCC dataset, a stronger agreement is obtained with the independent VOD-AGB and L-VOD data. The LPJ-GUESS simulations with the ESA-CCI data and the VOD datasets converge on the conclusion that LULCC have had a stronger negative impact on the trend in tropical forest sink than estimated with previous LULCC data. Thus, trends in contribution to the global terrestrial carbon sink of boreal and tropical forests diverge, and the main contributor to the global terrestrial carbon sink is observed to change from tropical to boreal forests over the study period.

Discussions

There is ongoing debate regarding the magnitude of the effect of CO_2 fertilization on the terrestrial carbon sink over recent decades. Experimental studies indicate increased growth rates under elevated CO_2 concentrations[29], whereas studies using tree-ring data claim that this effect is eliminated at larger spatial scales due to other constraining variables, such as nutrient limitation or water
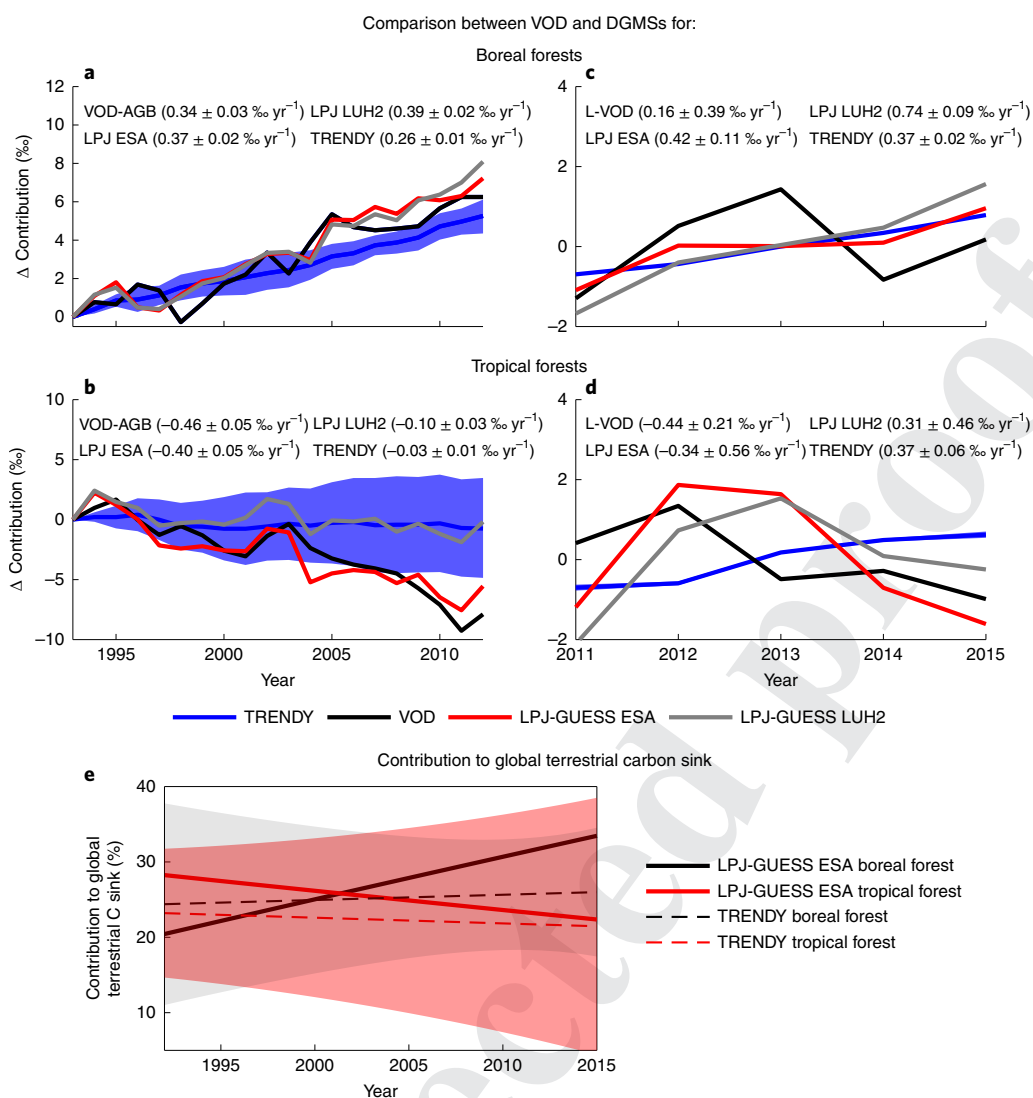
Fig. 5 | Comparison between model simulations using different land use and land cover change datasets. a–d, Net changes in biome contribution to global AGB obtained from model results with LPJ-GUESS with ESA-CCI, LPJ-GUESS with LUH2, TRENDY models with LUH2 (mean ± s.d.) and VOD-AGB (**a,b**), and L-VOD (**c,d**), for boreal forests (**a,c**) and (**b,d**) tropical forests. **e,** Change in contribution to the global terrestrial carbon sink for 1992–2015 for the boreal and tropical forests for the LPJ-GUESS simulations with the ESA-CCI land cover dataset and from the TRENDY model ensemble. The shaded areas indicate one standard deviation intervals of the TRENDY models.

stress[30]. Attempts to constrain the impact of CO_2 fertilization from large-scale observations point at an effect visible in the decrease of the growth rate of atmospheric growth rate of CO_2 during the hiatus period of stagnating global temperatures[31], although explanations for this, such as lower soil respiration[32] and decelerating land use emissions[33], have also been proposed. We see no decrease in LULCC emissions over the hiatus period (Supplementary Fig. 3b), indicating that decelerating land use emissions[33] do not explain the decrease of atmospheric CO_2 growth rate. Schimel et al.[8] compared bottom-up and top-down approaches of terrestrial carbon feedbacks in the context of the global mass balance, and found that up to 60% of the present-day terrestrial sink is caused by increasing atmospheric CO_2, in line with our results (Supplementary Table 9). They also showed that CO_2 fertilization is strongest in tropical regions, but additionally contributes to high-latitude enhancement of CO_2 uptake[8,34]. Sellers et al.[7] used a top-down approach assimilating in situ and satellite-based CO_2 concentration data into atmospheric transport models, which indicate a neutral carbon sink for the tropical forests, in contrast with a strong increase in the carbon

sink of the northern extra-tropics for 1990–2015. They hypothesized, in line with our results, that the carbon sink in intact tropical forests is nearly in balance with the net deforestation. We note that during the hiatus period of stagnating global temperatures[31,32], there was a strong increasing trend in VOD-AGB for the boreal forests (Fig. 2) and a persistent greening trend, indicated by satellite vegetation indices[35]. This persistent northern carbon sink is generally attributed to climate change and CO_2 fertilization effects, but forcing mechanisms are still considered to be a possibility[36–38].

The estimations of global carbon emissions and sinks require a combination of methods, measurements, data sources and models[12]; the importance of incorporating dynamic observation-based land cover data has long been recognized for documenting the role of terrestrial ecosystems[19]. Applying Earth observation-based LULCC data in a global DGVM reconciled model simulations with observed changes in AGB for 1993–2015 (from VOD-AGB and L-VOD) (Fig. 2), and provides a global carbon sink estimate that is in better agreement with the GCP atmospheric budget than models driven by the LUH2 dataset[28] (Supplementary Information, subsection 2.7).

The ESA-CCI land cover data has very different patterns of forested area compared with LUH2, and shows a larger global forested area and more negative trends for 1992–2015 (Supplementary Information, subsection 2.1). The results also show no trend of the sink for tropical forests, and a strong increasing trend for the boreal forest sink—that is, diverging trends in the contribution of these two biomes to the global terrestrial carbon sink.

However, LULCC in this study only include fluxes that are a result of natural and anthropogenic disturbances associated with a change in land cover classes within the ESA-CCI land cover product, thereby ignoring the effects of converting primary forest to managed secondary forest. For example, conversion of primary forest to oil palm and rubber plantations is still assigned to forests in the ESA-CCI dataset, even though it is associated with emissions from the loss of biomass and soil carbon. Changes in carbon density within land cover classes are also likely to take place and are not currently captured by the simulations. The strong negative trends in VOD-AGB and L-VOD for tropical forests (Fig. 2 and Supplementary Figs. 9 and 10) indeed indicate the occurrence of such land use transitions. The strong decline in the tropical forests carbon sink has previously been claimed by both Pan et al.[2], using forest inventory data, and by Baccini et al.[5], using optical Earth observation data, and has also been shown on plot scale for more than 300 plots in the Amazon region, where tree mortality led to a shortening of the carbon residence time[39]. Additionally, CO_2 inversions indicate a substantially larger carbon sink at high northern latitudes ($> 20°$ N) and either a source or neutral carbon exchange from the tropics and the south ($< 20°$ N)[7,8,40]. Incorporation of forest degradation, forestry and agricultural management, mechanistic simulations of fire and other forms of natural disturbances (pest outbreaks and storm events) in DGVM modelling is therefore essential to further improve our understanding of trends in carbon sinks and sources, and of the contribution of different biomes to changes within the global carbon cycle.

Methods

Land cover analysis. The dynamic global land cover dataset for 1992–2015 from ESA-CCI (spatial resolution of 0.0028°×0.0028°) was used in two different analyses: (1) to derive woody and herbaceous cover, for forcing the DGVM (see below), and (2) for separating the terrestrial Earth surface into its different biomes (as described below, points 2a-c).

In separating the terrestrial Earth surface: we applied a static Köppen climate classification of the Earth's surface with a spatial resolution of 0.1°×0.1° from Earthdata (https://earthdata.nasa.gov)[22] and used it for separation of the global land areas into different climate classes. We separated the global land area into the five main Köppen climate classes: Tropical (A), Arid (B), Temperate (C), Boreal (D), and Polar (E).

We used the dynamic global land cover dataset from ESA-CCI and divided the global land area into five different vegetation classes following Supplementary Table 1: forest, savannah/shrubland, crop/grassland, sparse vegetation and bare land.

We combined the vegetation and climate classes into ten different biomes following the settings in Supplementary Table 2: bare land, regions with sparse vegetation, tundra, boreal with low vegetation, boreal forests, temperate with low vegetation, temperate forests, drylands, tropical with low vegetation, and tropical forests.

This separation was used to partition the simulated global terrestrial carbon sink into the different biomes covering the Earth.

It should be mentioned that: (1) there is a risk of natural disturbance suppressing woody cover, causing an area to not be detected as a forest, even though this is a temporary phenomenon. This is a risk, but the processing chain of the ESA-CCI land cover data has been set up to avoid false change detection due to such interannual variability in the classifications. (2) The reliability of the ESA-CCI product can vary spatially depending on number of valid and cloud-free observations[15]. The lack of an estimate of the uncertainty is therefore a limitation.

DGVM LPJ-GUESS simulations. The DGVM LPJ-GUESS[23,41], developed for studies of vegetation dynamics and ecosystem biogeochemistry, was used to estimate the net terrestrial carbon exchanges. LPJ-GUESS is a terrestrial ecosystem model, combining a detailed representation of population dynamics with mechanistic descriptions of the plant physiological processes of carbon, nitrogen and water cycling. It has been subject to extensive evaluations of temporal and

spatial variation in ecosystem carbon balance at a range of spatial and temporal scales[3,42].

Monthly mean air temperature, precipitation and cloud cover (1901–2015) from Climate Research Unit time-series dataset 3.24.01[43], annual atmospheric CO_2 concentrations[44,45] and monthly nitrogen deposition[46] were applied to drive the model. The model was configured to run in cohort mode, in which age classes (cohorts) of prescribed plant functional types are simulated in patches. The plant functional types were set as in ref. [47]. Simulations were performed using 20 replicate patches in each grid cell and an average value of these 20 patches was calculated as output. Disturbances, representing pest outbreaks and storm events, were set up as stochastic events with an expected frequency of 0.01 yr^{-1} at patch level. In addition, wildfires were simulated based on fuel (litter) load, dryness and physical conditions. The first 30 yr of the observed meteorological data (1901–1930, with detrended temperatures) and the CO_2 concentration for 1901 were used repeatedly during a 500-yr-long spin-up phase. This was done in order to achieve a vegetation structure and ecosystem carbon and nitrogen pools in dynamic equilibrium with the long-term climate.

Because the ESA-CCI land cover dataset does not provide land use fractions directly, but rather land cover types, these land cover types were converted to fractions of woody cover following the settings in Supplementary Table 1. The woody fractions were then aggregated to the same resolution as the CRU data (0.5°×0.5°). The estimated fractions of woody cover for the starting year of the ESA-CCI data, 1992, were compared with simulated woody cover from LPJ-GUESS for the same year in a simulation with the meteorological forcing as described above, but without applying land use (also referred to as potential vegetation). On the basis of the difference between the simulated and the estimated fractions of woody cover, a land use correction was determined, which reduced the number of patches in which trees were allowed to grow to match the observed ESA-CCI-estimated cover for 1992. In cases where the ESA-CCI-estimated woody cover exceeded the value simulated in the no-land use simulation with LPJ-GUESS, no correction was applied.

The effects of meteorological forcing, biogeochemical drivers (CO_2 and N) and LULCC were determined from a set of factorial simulations, in which all except one of the drivers were kept at constant conditions resembling the period prior to 1992. These results were compared with a simulation with all drivers kept constant, and the differences between each of the factorial simulations and the all-constant simulation were attributed to the effect of these drivers.

Partitioning of the global-scale mean, trend and interannual variability in the terrestrial carbon sink to the different biomes. The mean global terrestrial carbon sink 1992–2015 was partitioned to the different biomes by summing the net ecosystem carbon exchange for each biome. To obtain the contribution per biome, each biome was divided by the global sum.

We estimated the trends for 1992–2015 by fitting ordinary least-squares linear regressions between both global and biome-level carbon sink using year as predictor. The biome contribution to the global trend was estimated by taking the absolute values of each specific biome trend divided by the sum of the absolute values of all biome trends. The absolute values were used to ensure that the trends added up to 100%, and since a contribution of small trends may otherwise become infinite.

We partitioned the contribution to the interannual variability of the terrestrial carbon sink of the different biomes (F_{IAV}) following the method in ref. [3]:

$$F_{IAV} = \frac{\sum_t \frac{x_{jt}|\mathbf{X}_t|}{\bar{\mathbf{X}}_t}}{\sum_t |\mathbf{X}_t|} \qquad (1)$$

where x_{jt} is the net carbon sink anomaly from long-term trend for a biome (j) and time (t; in yr); $\mathbf{X}_t$ is the anomaly of the global terrestrial carbon sink, so that $\mathbf{X}_t = \sum_j x_{jt}$. F_{IAV} is therefore the average relative anomaly weighted with the absolute anomaly of the global terrestrial carbon sink $|\mathbf{X}_t|$. The result indicates that biomes with high and low F_{IAV} contribute more or less to the interannual variability in the global terrestrial carbon sink.

Temporal changes in biome contributions to the global terrestrial carbon sink were estimated by making predictions of biome-level carbon sink on the basis of their respective trends and then annually dividing these predictions by the sum of all biome predictions.

Satellite passive microwave data. VOD derived from passive microwaves was found to be linearly related to vegetation water content[48] and time series of the yearly average of satellite-derived VOD products have been used for assessment of large-scale biomass dynamics[18,20]. Liu et al.[18] converted a satellite passive microwave derived VOD dataset for 1993–2012 to a time series of AGB on the basis of a relationship with AGB from ref. [49] The SMOS L-VOD dataset for 2011–2015 (v.105) used here was produced using the SMOS-IC algorithm[50].

First, L-VOD data for ascending (ASC) and descending (DESC) orbits were filtered according to the standard scene flags for strong topography, frozen soils (soil temperature < 273.5 K), urban areas and water bodies. We then applied a filter for effects of radio frequency interference by excluding data with a TB-RMSE index[20,50] higher than 6 K. We then applied a moving-average smoothing (window

size = 30 d) on the filtered ASC and DESC L-VOD time series[21]. We excluded outliers, corresponding to data lower (higher) than the 10th (90th) percentile of residues (being defined as differences between raw L-VOD data and smoothed L-VOD data). The filtered ASC and DESC L-VOD data were combined into one L-VOD dataset by keeping only the 30 L-VOD data points with the lowest TB-RMSE values. We then calculated the annual average L-VOD values, aggregated for each biome, and computed fractions against the average for 2011–2015. We kept the original L-VOD unit without converting into a biomass unit, given its rather linear relationship with static biomass carbon estimations[19,20,51].

The temporal changes in biome contributions to the global AGB were calculated by dividing each biome by the global sum. The changes in time were then assessed by calculating the difference for each year against the estimates of the first year in the time series (1993) for VOD-AGB, and against the mean estimates of the time series for L-VOD. Ordinary least-squares linear regression trends were fitted to these changes.

DGVM LPJ-GUESS simulations forced with the LUH2 land cover dataset. The DGVM simulations with LPJ-GUESS were repeated with the same settings as previously described except that the land cover dataset used for forcing the model was instead the LUH2 data[28]. We adopted the LUH2 data classes for the DGVM LPJ-GUESS by representing the cropland and pasture classes with grassland, barren and urban with bare land, and the remainder with natural vegetation, letting the model dynamically simulate the emergent vegetation cover.

TRENDY DGVM data. We compared our LPJ-GUESS simulations against output of DGVMs from the TRENDY model ensemble (v.5)[26,27]. LPJ-GUESS was excluded from the TRENDY model ensemble in order to not compare our simulations with the same DGVM. From remaining TRENDY models, we selected four (CABLE, DLEAM, ISAM and VEGAS) which fulfilled the criteria of (1) using LULCC forcing, and (2) having the same spatial resolution as the LPJ-GUESS simulations (0.5°). The selected models used Climate Research Unit-National Centers for Environmental Prediction v.7 dataset as meteorological forcing, global atmospheric CO_2 from ice core and National Oceanic and Atmospheric Administration annual resolution (1860–2015)[44,45], and land use forcing from the LUH2 data[28].

Reporting Summary. Further information on research design is available in the Nature Research Reporting Summary linked to this article.

Data availability

Data from the ESA-CCI land cover dataset is freely available from ESA-CCI (http://www.esa-landcover-cci.org/?q=node/169)[15]. The Köppen climate classification is freely available at https://earthdata.nasa.gov. The LPJ-GUESS simulated terrestrial carbon exchange estimates, the simulated AGB data, the fractions of woody, herbaceous and bares land, and the annual SMOS L-VOD data are available at https://doi.org/10.17894/ucph.7a8d3a3c-6056-445b-b05c-4212231aff40. The VOD-AGB dataset derived over the period 1993–2012 can be accessed at http://www.wenfo.org/wald/global-biomass[18]. For the TRENDY data, please see http://dgvm.ceh.ac.uk/node/21/.

Code availability

The codes used in the data analysis is available at https://doi.org/10.17894/ucph.7a8d3a3c-6056-445b-b05c-4212231aff40. The codes are: 1) the code used for converting the ESA-CCI land cover to fractions of woody, herbaceous and bares land; 2) the codes used for separating the terrestrial Earth surface into its different biomes; 3) the codes used for partitioning the global-scale mean, trend and interannual variability in the terrestrial carbon sink to the different biomes; and 4) the codes used for the factorial simulations.

References

1. Le Quéré, C. et al. Global carbon budget 2018. *Earth Syst. Sci. Data* **10**, 2141–2194 (2018).
2. Pan, Y. et al. A large and persistent carbon sink in the world's forests. *Science* **333**, 988–993 (2011).
3. Ahlström, A. et al. The dominant role of semi-arid ecosystems in the trend and variability of the land CO_2 sink. *Science* **348**, 895–899 (2015).
4. Ciais, P. et al. Five decades of northern land carbon uptake revealed by the interhemispheric CO_2 gradient. *Nature* **568**, 221–225 (2019).
5. Baccini, A. et al. Tropical forests are a net carbon source based on aboveground measurements of gain and loss. *Science* **358**, 230–234 (2017).
6. Peylin, P. et al. Global atmospheric carbon budget: results from an ensemble of atmospheric CO_2 inversions. *Biogeosciences* **10**, 6699–6720 (2013).
7. Sellers, P. J., Schimel, D. S., Moore, B., Liu, J. & Eldering, A. Observing carbon cycle–climate feedbacks from space. *Proc. Natl Acad. Sci. USA* **115**, 7860–7868 (2018).
8. Schimel, D., Stephens, B. B. & Fisher, J. B. Effect of increasing CO_2 on the terrestrial carbon cycle. *Proc. Natl Acad. Sci. USA* **112**, 436–441 (2015).
9. Palmer, P. I. et al. Net carbon emissions from African biosphere dominate pan-tropical atmospheric CO_2 signal. *Nat. Commun.* **10**, 3344 (2019).
10. Krausmann, F. et al. Global socioeconomic material stocks rise 23-fold over the 20th century and require half of annual resource use. *Proc. Natl Acad. Sci. USA* **114**, 1880–1885 (2017).
11. Rockström, J. et al. A safe operating space for humanity. *Nature* **461**, 472 (2009).
12. Steffen, W. et al. Planetary boundaries: Guiding human development on a changing planet. *Science* **347**, 1259855 (2015).
13. Erb, K.-H. et al. Land management: data availability and process understanding for global change studies. *Glob. Change Biol.* **23**, 512–533 (2017).
14. Erb, K.-H. et al. Biomass turnover time in terrestrial ecosystems halved by land use. *Nat. Geosci.* **9**, 674–678 (2016).
15. ESA. *CCI Land Cover Map* http://www.esa-landcover-cci.org/?q=node/169 (2017).
16. Bontemps, S. et al. Revisiting land cover observation to address the needs of the climate modeling community. *Biogeosciences* **9**, 2145–2157 (2012).
17. Li, W. et al. Gross and net land cover changes in the main plant functional types derived from the annual ESA CCI land cover maps (1992–2015). *Earth Syst. Sci. Data* **10**, 219–234 (2018).
18. Liu, Y. Y. et al. Recent reversal in loss of global terrestrial biomass. *Nat. Clim. Change* **5**, 470–474 (2015).
19. Rodríguez-Fernández, N. J. et al. An evaluation of SMOS L-band vegetation optical depth (L-VOD) data sets: high sensitivity of L-VOD to above-ground biomass in Africa. *Biogeosciences* **15**, 4627–4645 (2018).
20. Brandt, M. et al. Satellite passive microwaves reveal recent climate-induced carbon losses in African drylands. *Nat. Ecol. Evol.* **2**, 827–835 (2018).
21. Tian, F. et al. Coupling of ecosystem-scale plant water storage and leaf phenology observed by satellite. *Nat. Ecol. Evol.* **2**, 1428–1435 (2018).
22. Peel, M. C., Finlayson, B. L. & McMahon, T. A. Updated world map of the Koppen–Geiger climate classification. *Hydrol. Earth Syst. Sci.* **11**, 1633–1644 (2007).
23. Smith, B. et al. Implications of incorporating N cycling and N limitations on primary production in an individual-based dynamic vegetation model. *Biogeosciences* **11**, 2027–2054 (2014).
24. Zeng, N. et al. Causes and impacts of the 2005 Amazon drought. *Environ. Res. Lett.* **3**, 014002 (2008).
25. Lewis, S. L., Brando, P. M., Phillips, O. L., van der Heijden, G. M. F. & Nepstad, D. The 2010 Amazon drought. *Science* **331**, 554–554 (2011).
26. Sitch, S. et al. Evaluation of the terrestrial carbon cycle, future plant geography and climate-carbon cycle feedbacks using five Dynamic Global Vegetation Models (DGVMs). *Glob. Change Biol.* **14**, 2015–2039 (2008).
27. Sitch, S. et al. Recent trends and drivers of regional sources and sinks of carbon dioxide. *Biogeosciences* **12**, 653–679 (2015).
28. Hurtt, G. C. et al. Harmonization of land-use scenarios for the period 1500–2100: 600 years of global gridded annual land-use transitions, wood harvest, and resulting secondary lands. *Clim. Change* **109**, 117 (2011).
29. Gifford, R. M. The CO_2 fertilising effect—does it occur in the real world? *New Phytol.* **163**, 221–225 (2004).
30. Hararuk, O., Campbell, E. M., Antos, J. A. & Parish, R. Tree rings provide no evidence of a CO_2 fertilization effect in old-growth subalpine forests of western Canada. *Glob. Change Biol.* **25**, 1222–1234 (2019).
31. Keenan, T. F. et al. Recent pause in the growth rate of atmospheric CO_2 due to enhanced terrestrial carbon uptake. *Nat. Commun.* **7**, 13428 (2016).
32. Ballantyne, A. et al. Accelerating net terrestrial carbon uptake during the warming hiatus due to reduced respiration. *Nat. Clim. Change* **7**, 148 (2017).
33. Piao, S. et al. Lower land-use emissions responsible for increased net land carbon sink during the slow warming period. *Nat. Geosci.* **11**, 739–743 (2018).
34. Wenzel, S., Cox, P. M., Eyring, V. & Friedlingstein, P. Projected land photosynthesis constrained by changes in the seasonal cycle of atmospheric CO_2. *Nature* **538**, 499–501 (2016).
35. Winkler, A. J., Myneni, R. B., Alexandrov, G. A. & Brovkin, V. Earth system models underestimate carbon fixation by plants in the high latitudes. *Nat. Commun.* **10**, 885 (2019).
36. Lucht, W. et al. Climatic control of the high-latitude vegetation greening trend and Pinatubo effect. *Science* **296**, 1687–1689 (2002).
37. Piao, S., Friedlingstein, P., Ciais, P., Zhou, L. & Chen, A. Effect of climate and CO_2 changes on the greening of the Northern Hemisphere over the past two decades. *Geophys. Res. Lett.* **33**, L23402 (2006).
38. Graven, H. D. et al. Enhanced seasonal exchange of CO_2 by northern ecosystems since 1960. *Science* **341**, 1085–1089 (2013).
39. Brienen, R. J. W. et al. Long-term decline of the Amazon carbon sink. *Nature* **519**, 344 (2015).
40. Gaubert, B. et al. Global atmospheric CO_2 inverse models converging on neutral tropical land exchange, but disagreeing on fossil fuel and atmospheric growth rate. *Biogeosciences* **16**, 117–134 (2019).

41. Smith, B., Prentice, I. C. & Sykes, M. T. Representation of vegetation dynamics in the modelling of terrestrial ecosystems: comparing two contrasting approaches within European climate space. *Glob. Ecol. Biogeogr.* **10**, 621–637 (2001).

42. Piao, S. et al. Evaluation of terrestrial carbon cycle models for their response to climate variability and to CO_2 trends. *Glob. Change Biol.* **19**, 2117–2132 (2013).

43. Harris, I., Jones, P. D., Osborn, T. J. & Lister, D. H. Updated high-resolution grids of monthly climatic observations—the CRU TS3.10 dataset. *Int. J. Clim.* **34**, 623–642 (2014).

44. Etheridge, D. M. et al. Natural and anthropogenic changes in atmospheric CO_2 over the last 1,000 years from air in Antarctic ice and firn. *J. Geophys. Res.* **101**, 4115–4128 (1996).

45. Keeling, C. D., Whorf, T. P., Wahlen, M. & van der Plicht, J. Interannual extremes in the rate of rise of atmospheric carbon dioxide since 1980. *Nature* **375**, 666–670 (1995).

46. Lamarque, J.-F. et al. Historical (1850–2000) gridded anthropogenic and biomass burning emissions of reactive gases and aerosols: methodology and application. *Atmos. Chem. Phys.* **10**, 7017–7039 (2010).

47. Ahlström, A., Miller, P. A. & Smith, B. Too early to infer a global NPP decline since 2000. *Geophys. Res. Lett.* **39**, L15403 (2012).

48. Jackson, T. J. & Schmugge, T. J. Vegetation effects on the microwave emission of soils. *Remote Sens. Environ.* **36**, 203–212 (1991).

49. Saatchi, S. S. et al. Benchmark map of forest carbon stocks in tropical regions across three continents. *Proc. Nat. Acad. Sci. U. S. A.* **108**, 9899–9904 (2011).

50. Fernandez-Moran, R. et al. SMOS-IC: an alternative SMOS soil moisture and vegetation optical depth product. *Remote Sens.* **9**, 457 (2017).

51. Fan, L. et al. Satellite-observed pantropical carbon dynamics. *Nat. Plants* **5**, 944–951 (2019).

Acknowledgements

Author contributions

Competing interests

The authors declare no competing interests.

Additional information

Supplementary information is available for this paper at https://doi.org/10.1038/s41559-019-1090-0.

Correspondence and requests for materials should be addressed to T.T.

Reprints and permissions information is available at www.nature.com/reprints.

Publisher's note Springer Nature remains neutral with regard to jurisdictional claims in published maps and institutional affiliations.

QUERY FORM

AUTHOR:

The following queries have arisen during the editing of your manuscript. Please answer by making the requisite corrections directly in the e.proofing tool rather than marking them up on the PDF. This will ensure that your corrections are incorporated accurately and that your paper is published as quickly as possible.

Query No.	Nature of Query
Q1:	Please confirm or correct the city name inserted in affiliation 5.
Q2:	Please confirm that the edits to the sentence 'Tropical and boreal forests contributed equally….' preserve the originally intended meaning.
Q3:	Please check your article carefully, coordinate with any co-authors and enter all final edits clearly in the eproof, remembering to save frequently. Once corrections are submitted, we cannot routinely make further changes to the article.
Q4:	Note that the eproof should be amended in only one browser window at any one time; otherwise changes will be overwritten.
Q5:	Author surnames have been highlighted. Please check these carefully and adjust if the first name or surname is marked up incorrectly. Note that changes here will affect indexing of your article in public repositories such as PubMed. Also, carefully check the spelling and numbering of all author names and affiliations, and the corresponding email address(es).
Q6:	You cannot alter accepted Supplementary Information files except for critical changes to scientific content. If you do resupply any files, please also provide a brief (but complete) list of changes. If these are not considered scientific changes, any altered Supplementary files will not be used, only the originally accepted version will be published.
Q7:	Reworded the fragment '(low vegetation being areas...)'. OK?
Q8:	Please check consistency between Figs. 2 and 3: semi-arid vs dryland.
Q9:	In the sentence 'Attempts to constrain...', please confirm or correct 'growth rate of atmospheric growth rate of CO_2'.
Q10:	The link to the Earthdata website was moved from the reference list to the text per style. We can only use links to specific pages within a website in the reference list. If referring to the website as a whole, they must be cited as a link in the text.
Q11:	We conform to the style that vectors are set in bold roman font. The magnitude of a vector is set innonbold italics, as are scalar components, tensors and matrices. Please ensure your text is consistent withthis throughout.
Q12:	Please expand TB-RMSE.
Q13:	Please expand/define the acronyms CABLE, DLEAM, ISAM and VEGAS.

nature research

Corresponding author(s):   Torbern Tagesson

Last updated by author(s):   Dec 18, 2019

Reporting Summary

Nature Research wishes to improve the reproducibility of the work that we publish. This form provides structure for consistency and transparency in reporting. For further information on Nature Research policies, see Authors & Referees and the Editorial Policy Checklist.

Statistics

For all statistical analyses, confirm that the following items are present in the figure legend, table legend, main text, or Methods section.

n/a	Confirmed	
☒	☐	The exact sample size (*n*) for each experimental group/condition, given as a discrete number and unit of measurement
☒	☐	A statement on whether measurements were taken from distinct samples or whether the same sample was measured repeatedly
☐	☒	The statistical test(s) used AND whether they are one- or two-sided *Only common tests should be described solely by name; describe more complex techniques in the Methods section.*
☒	☐	A description of all covariates tested
☒	☐	A description of any assumptions or corrections, such as tests of normality and adjustment for multiple comparisons
☐	☒	A full description of the statistical parameters including central tendency (e.g. means) or other basic estimates (e.g. regression coefficient) AND variation (e.g. standard deviation) or associated estimates of uncertainty (e.g. confidence intervals)
☒	☐	For null hypothesis testing, the test statistic (e.g. *F*, *t*, *r*) with confidence intervals, effect sizes, degrees of freedom and *P* value noted *Give P values as exact values whenever suitable.*
☒	☐	For Bayesian analysis, information on the choice of priors and Markov chain Monte Carlo settings
☒	☐	For hierarchical and complex designs, identification of the appropriate level for tests and full reporting of outcomes
☐	☒	Estimates of effect sizes (e.g. Cohen's *d*, Pearson's *r*), indicating how they were calculated

Our web collection on statistics for biologists contains articles on many of the points above.

Software and code

Policy information about availability of computer code

Data collection	No software was used for data collection.
Data analysis	Data processing was performed in Matlab 2017b. The scripts are publicly available at http://doi.org/10.17894/ucph.7a8d3a3c-6056-445b-b05c-4212231aff40.

For manuscripts utilizing custom algorithms or software that are central to the research but not yet described in published literature, software must be made available to editors/reviewers. We strongly encourage code deposition in a community repository (e.g. GitHub). See the Nature Research guidelines for submitting code & software for further information.

Data

Policy information about availability of data

All manuscripts must include a data availability statement. This statement should provide the following information, where applicable:

- Accession codes, unique identifiers, or web links for publicly available datasets
- A list of figures that have associated raw data
- A description of any restrictions on data availability

Data from the ESA-CCI land cover dataset is freely available from ESA-CCI (http://www.esa-landcover-cci.org/?q=node/169)15. The Köppen climate classification is freely available at https://earthdata.nasa.gov41. The LPJ-GUESS simulated terrestrial carbon exchange estimates, the simulated aboveground biomass data, the fractions of woody, herbaceous and bares land, and the annual SMOS L-VOD data are available at http://doi.org/10.17894/ucph.7a8d3a3c-6056-445b-b05c-4212231aff40. The VOD-AGB data set derived over the period 1993–2012 can be accessed at http://www.wenfo.org/wald/global-biomass18. For the TRENDY data, please see http://dgvm.ceh.ac.uk/node/21/.

Field-specific reporting

Please select the one below that is the best fit for your research. If you are not sure, read the appropriate sections before making your selection.

☐ Life sciences　　　☐ Behavioural & social sciences　　　☒ Ecological, evolutionary & environmental sciences

For a reference copy of the document with all sections, see nature.com/documents/nr-reporting-summary-flat.pdf

Ecological, evolutionary & environmental sciences study design

All studies must disclose on these points even when the disclosure is negative.

Study description	We assimilated the first dynamic long-term (>20 years) Earth observation-based global land cover dataset into a dynamic global vegetation model to better represent the impacts of land use and land cover changes on biome-aggregated net terrestrial carbon sinks.
Research sample	The dynamic global land cover data set 1992-2015 from the European Space Agency (ESA) Climate Change Initiative (CCI) (spatial resolution of 0.0028×0.0028°) was used in the analyses. The dynamic global land cover product for 1992-2015 (from the European Space Agency (ESA) Climate Change Initiative (CCI)) is the first detailed long term (>20 years) time series of land cover based on state-of-the-art moderate resolution Earth observation data and thereby provides a timely opportunity to perform data-informed modelling of the role of LULCC on terrestrial carbon sink/sources.
Sampling strategy	The dynamic global land cover dataset 1992-2015 from the ESA-CCI was used for separating the terrestrial Earth surface into its different biomes: (1) we applied a static Köppen climate classification of the Earth's surface with a spatial resolution of 0.1×0.1° and used it for separation of the global land areas into different climate classes. We separated the global land area into the five main Köppen climate classes: Tropical (A), Arid (B), Temperate (C), Boreal (D), and Polar (E). (2) We used the dynamic global land cover dataset from ESA-CCI and divided the global land area into 5 different vegetation classes forest, savannah/shrubland, crop/grassland, sparse vegetation, and bare land. (3)We combined the vegetation and climate classes into 10 different biomes: bare land, regions with sparse vegetation, tundra, boreal with low vegetation, boreal forests, temperate with low vegetation, temperate forests, drylands, tropical with low vegetation, and tropical forests. All pixels within the different biomes were used.
Data collection	We use freely available data from European Space Agency (ESA) Climate Change Initiative (CCI).
Timing and spatial scale	Freely available land cover data is available from 1992-2015, and this is also the study period used.
Data exclusions	No data were excluded.
Reproducibility	Vegetation optical depth (VOD) derived from passive microwaves was used for verifying the experimental findings. Liu et al. converted a satellite passive microwave derived VOD dataset 1993-2012 to a time series of aboveground biomass (AGB) based on a relationship with AGB. The Soil Moisture and Ocean Salinity (SMOS) L-VOD dataset 2011-2015 (version 105) was also used here.
Randomization	Randomization was not applied in this study.
Blinding	Blinding is not relevant for our study as we used well-defined criteria for biome grouping and included all the valid observations within each biome.

Did the study involve field work?　　☐ Yes　　☒ No

Reporting for specific materials, systems and methods

We require information from authors about some types of materials, experimental systems and methods used in many studies. Here, indicate whether each material, system or method listed is relevant to your study. If you are not sure if a list item applies to your research, read the appropriate section before selecting a response.

Materials & experimental systems

n/a	Involved in the study
☒	☐ Antibodies
☒	☐ Eukaryotic cell lines
☒	☐ Palaeontology
☒	☐ Animals and other organisms
☒	☐ Human research participants
☒	☐ Clinical data

Methods

n/a	Involved in the study
☒	☐ ChIP-seq
☒	☐ Flow cytometry
☒	☐ MRI-based neuroimaging